J Appl Electrochem (2008) 38:973–978
DOI 10.1007/s10800-008-9510-x

ORIGINAL PAPER

New electrocatalytic materials based on mixed metal oxides: electrochemical quartz crystal microbalance characterization

A. Vertova · L. Borgese · G. Cappelletti · C. Locatelli · A. Minguzzi · C. Pezzoni · S. Rondinini

Received: 13 September 2007 / Revised: 30 January 2008 / Accepted: 31 January 2008 / Published online: 19 February 2008

Abstract An electrochemical Quartz Crystal Microbalance (EQCM) was used to characterize a mixed metal oxide electrocatalyst, $Ir_{0.15}Sn_{0.85}O_2$, for the Oxygen Evolution Reaction (OER) in acidic medium in the potential range of the pseudo-capacitance reaction, from 0.4 to 1.2 V versus Reversible Hydrogen Electrode (RHE). The EQCM gold tip was characterized in H_2SO_4 0.05 M and $HClO_4$ 0.1 M. Subsequently, $Ir_{0.15}Sn_{0.85}O_2$ powder, synthesized by a sol–gel route, was supported on the tip gold surface for investigations in the same media. The simultaneous measurements of mass variation and current density as functions of potential led to the identification of the chemical species involved in the mass transfer between the oxide and the acidic solution during the pseudo-capacitance reaction.

Keywords EQCM · Oxygen electrocatalyst · Oxygen evolution reaction · Iridium

1 Introduction

Fossil fuel consumption and global climate changes [1] in connection with air pollution have prompted research for alternative and clean energy sources [2–5]. The challenging theme of the "hydrogen economy" [6–10] has experienced a wide interest due to the possibility of direct conversion between chemical and electrical energy through an electrochemical reaction, a truly "green process". Since hydrogen is an energy carrier and it is not directly available in nature, the energy conversion is a "green process" only if hydrogen is produced using non-fossil primary energy sources, e.g. through electrochemical processes [11]. These are of particular interest due to their intrinsic harmless operational conditions and low running costs, provided that renewable energy sources, such as solar or wind energy [12–14], can be used to supply electricity to the electrolyser. Up to now, industrial water electrolysis has been carried out in aqueous media containing an alkaline electrolyte, a mature and robust technology that nonetheless presents some disadvantages, mainly safety issues, due to the presence of caustic media, and low specific production rates combined with the necessity of hydrogen purification from alkaline "fogs". Recently, water electrolysis in acidic media, using demineralized water and polymer electrolyte membranes (PEM) in an arrangement similar to that of fuel cell systems, has gained interest for several reasons: greater safety and reliability, high operating current density and efficiency and construction simplicity [15, 16].

In this context, the development of new electrocatalytic materials for the OER is necessary both for improving the anode chemical stability in acidic medium and for reducing power consumption [15].

Since the 1970s, with the introduction of Dimensionally Stable Anodes, DSA®, in the chloralkali process, studies on noble metal oxide electrodes have led to the development of new electrocatalytic materials both for the OER [15, 17] and for the Hydrogen Evolution Reaction (HER) in acidic media [18]. It was demonstrated that among noble metal

A. Vertova (✉) · L. Borgese · G. Cappelletti · C. Locatelli · A. Minguzzi · C. Pezzoni · S. Rondinini
Department of Physical Chemistry and Electrochemistry, University of Milan, via Golgi 19, 20133 Milan, Italy
e-mail: alberto.vertova@unimi.it

Present Address:
L. Borgese
Department of Mechanical and Industrial Engineering, The University of Brescia, Via Branze 38, 25123 Brescia, Italy

Present Address:
C. Pezzoni
Industrie De Nora SpA, Via Bistolfi 35, 20134 Milan, Italy

oxides IrO_2 has good corrosion resistance in strong acidic solutions [19, 20], even though its activity is slightly lower than RuO_2 and its cost is prohibitive for industrial applications. However, new composite materials, based on IrO_2 dispersed in a less costly metal oxide as matrix, can lead to the development of new electrodes with good chemical resistance to the acidic environment and good electronic conductivity [17, 21]. A large number of oxidic systems have been obtained by changing the dispersing agent, the metal, the synthetic procedure and the mass ratio between components [17, 21–29].

Our research group has recently synthesized nanocrystalline binary (Ir + Sn) and ternary (Ir + Sn + Ta) mixed oxides based on SnO_2 as dispersing matrix [30, 31]. The sol–gel synthetic methodology was chosen for all materials, since this technique allows definition of, a priori, morphology, bulk and surface composition of the oxides by controlling the synthesis parameters. Both SnO_2–IrO_2 [32, 33] and SnO_2–IrO_2–Ta_2O_5 [34] mixtures, the latter exhibiting Ir enrichment at the nanoparticle surfaces, are very stable under prolonged O_2 evolution. In addition to this, electrodes containing more than 10% of precious metal oxide have kinetic parameters very similar to those of pure IrO_2, in acidic media [17, 27]. Therefore the selected stoichiometry, $Ir_{0.15}Sn_{0.85}O_2$, offers the possibility of retaining good electrode performances while reducing the Ir content.

In this paper, SnO_2–IrO_2 nanoparticles were characterized by Cyclic Voltammetry (CV) and also with Electrochemical Quartz Crystal Microbalance (EQCM) measurements. In particular, chemical species involved in the pseudo-capacitance reaction,

$$MeO_x(OH)_y + \delta e^- + \delta H^+ \rightleftarrows MeO_{x-\delta}(OH)_{y+\delta} \quad (1)$$

which can modify the oxide surface [34, 35], were investigated by cycling the electrode between 0.4 and 1.2 V versus the Reversible Hydrogen Electrode (RHE) and by coupling CV experiments with QCM measurements. The results suggest the presence of the Ir(III)/Ir(IV) transition, characterized by a wide peak at 0.9 V, and show that the hydrated proton is the exchanged chemical species during the charge/discharge capacitive process, thus emphasizing the importance of the hydration level of the powder.

2 Experimental

All the chemicals were of reagent grade purity and were used without further purification; doubly distilled water passed through a Milli-Q® apparatus was used to prepare solutions and suspensions.

2.1 Electrode preparation

SnO_2–IrO_2 electrocatalytic nanoparticles were prepared as described elsewhere [30–32, 34], from $Sn(C_4H_9O)_4$ and $IrCl_3{\cdot}3H_2O$ salt precursors, in order to obtain the $Ir_{0.15}Sn_{0.85}O_2$ mixture. The specific surface area of the powder was 80 $m^2\ g^{-1}$, determined by the classical BET procedure using a Coulter SA 3100 apparatus. The average diameter of the crystallites, $<d> = 4$ nm, was estimated using the Scherrer equation from the most intense reflection (101) of the SnO_2 cassiterite phase obtained on the basis of room temperature X-ray powder diffraction (XRPD). By elaborating the crystallite size a "calculated" surface area of 215 $m^2\ g^{-1}$ can be obtained. By comparing the calculated surface area with the experimental one a relevant degree of aggregation/sintering between the primary particles is expected. SEM pictures (see Fig. 1) confirmed that the particles are actually round-shaped aggregates of 10–20 nm diameter.

To perform EQCM tests, the calcinated powder was suspended in Milli-Q water (0.37 g dm^{-3}) using an ultrasonic bath for 30 min. Seventeen microliter suspension drops (sampled under sonication) were deposited on the tip gold surface. The tip was dried in air until complete solvent evaporation. This procedure allows sampling of the finer fraction of the powder, thus ensuring a highly homogeneous particle size distribution of the deposits.

2.2 Instrumentation

The electrochemical properties were investigated using a Picobalance V3.0 microbalance (Technobiochip, Italy), whose oscillator was a planar AT-cut quartz crystal (ICM, OK, USA) partially covered with sputtered gold (geometric area = 0.20 cm^2) and operated at a resonant frequency of 10 MHz, measured with an accuracy of 1 Hz. According to

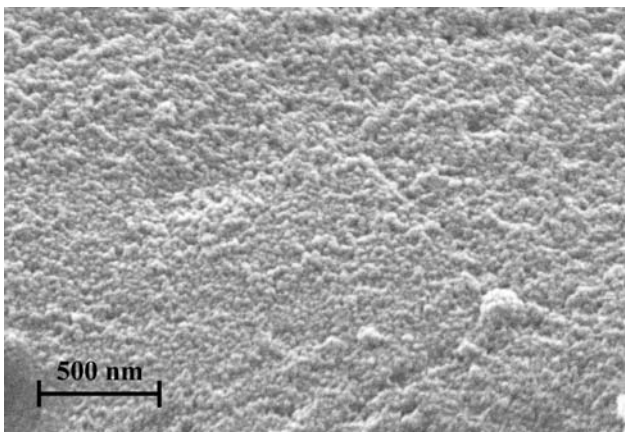

Fig. 1 SEM micrograph of $Ir_{0.15}Sn_{0.85}O_2$ powder

the Sauerbrey equation [36], frequency was converted into mass variation (Δm) by means of a numerical constant, which was determined through Ag deposition/dissolution chronopotentiometric experiments as described by Conway [37]. The value of the calibration constant obtained was 4.9 ± 0.4 ng Hz^{-1} cm^{-2}. The tip was connected to an AMEL 551 potentiostat/galvanostat coupled with an AMEL 566 function generator. All signals were recorded with a CIO-DAS1402/16 acquisition PC-board (Measurement Computing Corp.) and were treated by CorrWare (Scribner Associates, NC, USA). The filtering procedure of the EQCM data [38] was performed using Origin 6.0 software (OriginLab Corp., MA, USA).

Measurements were carried out in a 3-electrode cell equipped with a Pt counter-electrode and a Saturated Calomel Electrode (SCE), periodically calibrated against a Reversible Hydrogen Electrode (RHE) to which all quoted potentials are referred. All measurements were carried out in 0.05 M H_2SO_4 and 0.1 M $HClO_4$ solutions, previously degassed by N_2 bubbling, in the potential windows 0.4/1.2 or 0.4/1.7 V (RHE).

3 Results and discussion

EQCM bare gold tips were studied into two different electrolyte solutions, H_2SO_4 0.05 M and $HClO_4$ 0.1 M, using two potential ranges: 0.4–1.2 and 0.4–1.7 V versus RHE. While the former potential range is typically used for the electrochemical characterization of Ir-based oxide electrocatalysts [15, 34, 39], since it embraces the region of the pseudo-capacitive reaction, the latter is chosen in order to verify the behaviour of our EQCM tips in comparison with literature data. Our gold tips, studied in the widest potential range, present the well-known features of anion adsorption, concurrent anion expulsion and oxide formation, and phase-oxide growth [40, 41]. These processes are evident in Fig. 2, which shows CV and frequency variation (frequency decrease corresponds to weight increase) versus potential, recorded simultaneously, of an as received gold tip in H_2SO_4 0.05 M. The CVs obtained in $HClO_4$ 0.1 M are similar to those described in [40]. The different changes in frequency variation (Fig. 2 right axis) during the potential scan are evidence of the described phenomena [40]. By limiting the positive end-point to 1.2 V, the only evident process is the adsorption/desorption of sulphate anions (see Fig. 3a), which takes place in the 0.8–0.9 V interval. It is worthwhile underlining that this feature is not appreciable unless the tip is electrochemically activated by preliminary cycling up to 1.7 V, during which the formation and successive reduction of oxide layer(s) provide a reproducibly reconstructed gold surface [42]. In the absence of the electrochemical etching or just 1 day after the treatment, irrespective of storing the tip either in air or

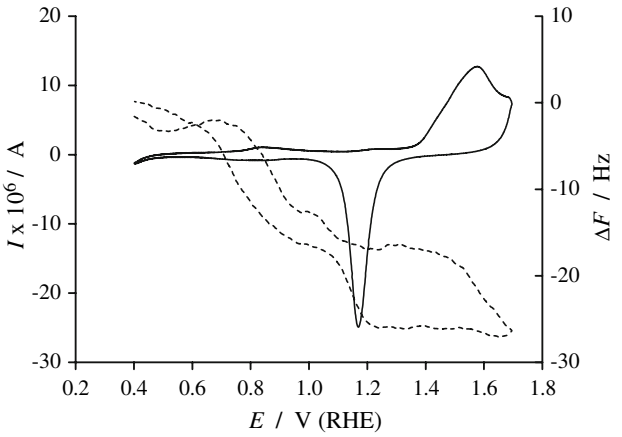

Fig. 2 Current intensity (left axis, full line) and frequency variation (right axis, dashed line) versus E characteristics, recorded simultaneously, of a gold tip in H_2SO_4 0.05 M; scan rate 20 mV s^{-1}

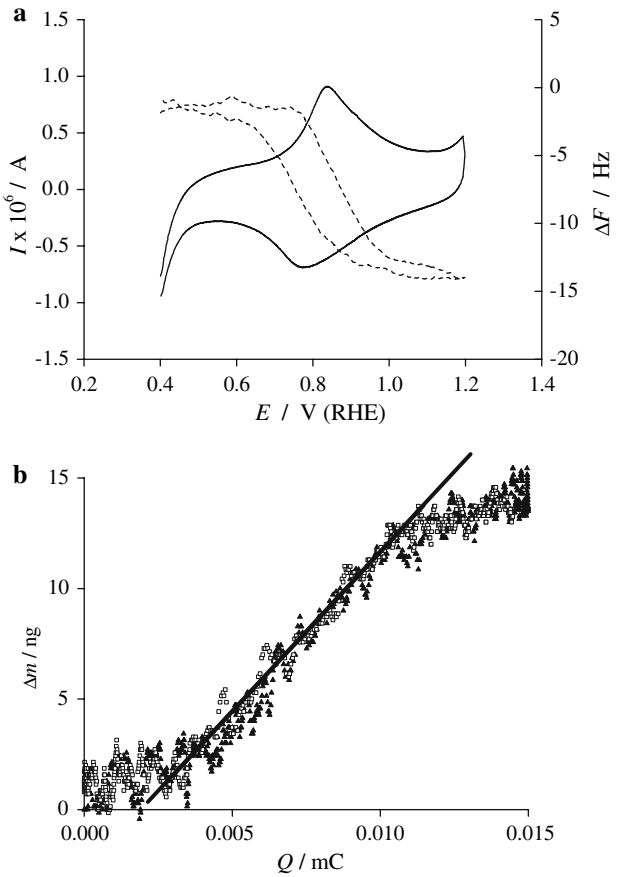

Fig. 3 (**a**) Current intensity (left axis, full line) and frequency variation (right axis, dashed line) versus E characteristics, recorded simultaneously, of a gold tip in H_2SO_4 0.05 M after CV presented in Fig. 2; scan rate 20 mV s^{-1}. (**b**) Mass variation (Δm) versus cumulative charge (Q) obtained by integrating the CV of Fig. 3a; empty squares: anodic scan; full triangles: cathodic scan

water, the adsorption/desorption features of both current and frequency signals are completely lost, thus pointing to the deactivation of the gold sites on which sulphate anions can adsorb.

It is possible to investigate the adsorption/desorption process by means of a mass to charge ratio analysis, by integrating CVs, from 0.4 to 1.2 V, and coupling the calculated charge (Q) with the mass variation (Δm) obtained from EQCM measurements. Figure 3b shows mass variation (Δm) versus cumulative charge (Q), calculated by integrating the CV represented in Fig. 3a. Mass and charge show a linear relationship, whose slope of 1430 ng mC^{-1} corresponds to a variation of 138 g (mol of electrons)$^{-1}$, which can be justified by the injection (anodic sweep)/expulsion (cathodic sweep) of 1 mol of doubly hydrated HSO_4^- per mole of electrons [40]. As already discussed, this process is operative only on a freshly activated surface. Likewise, anion adsorption in $HClO_4$ 0.1 M requires the etching procedure.

When $Ir_{0.15}Sn_{0.85}O_2$ is deposited on the gold tip surface a large increase in current is obtained, both in H_2SO_4 and $HClO_4$ solutions, due to the roughness of the electrocatalytic deposit. Broad peaks, connected with the pseudo-capacitance reaction, appear at typical potentials between 0.8 and 0.9 V versus RHE [23, 39, 43], Fig. 4 in 0.05 M H_2SO_4.

When the frequency variation is concomitantly recorded (Fig. 5a) a mass increase (frequency decrease) is observed up to 1 V, followed by a decrease at higher potentials. Mass variation (Δm) versus cumulative charge (Q), obtained by integrating the CV of Fig. 5a, is presented in Fig. 5b (anodic scan): two trends are clearly visible. Up to 0.05 mC the curve shows a slope of 271 ng mC^{-1}, resulting in a mass increase of 26 g (mol of electrons)$^{-1}$. This trend can be explained by the injection of 1 mol of SO_4^{2-} (theoretically + 48 g (mol of electrons)$^{-1}$) and the

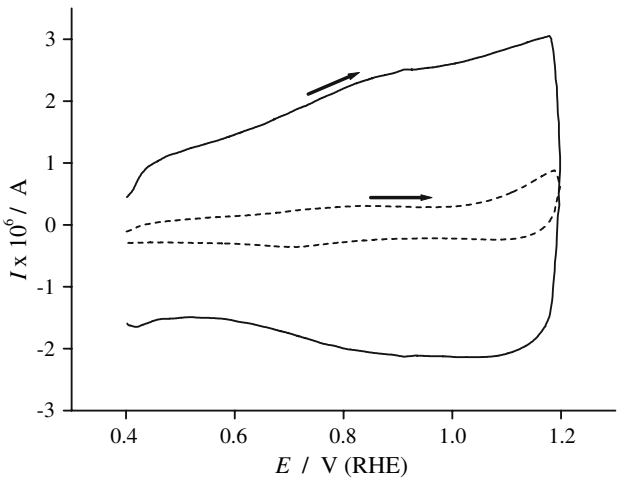

Fig. 4 CVs of a bare gold tip (dashed line) and of a tip covered with $Ir_{0.15}Sn_{0.85}O_2$ (full line) in H_2SO_4 0.05 M; scan rate 20 mV s^{-1}

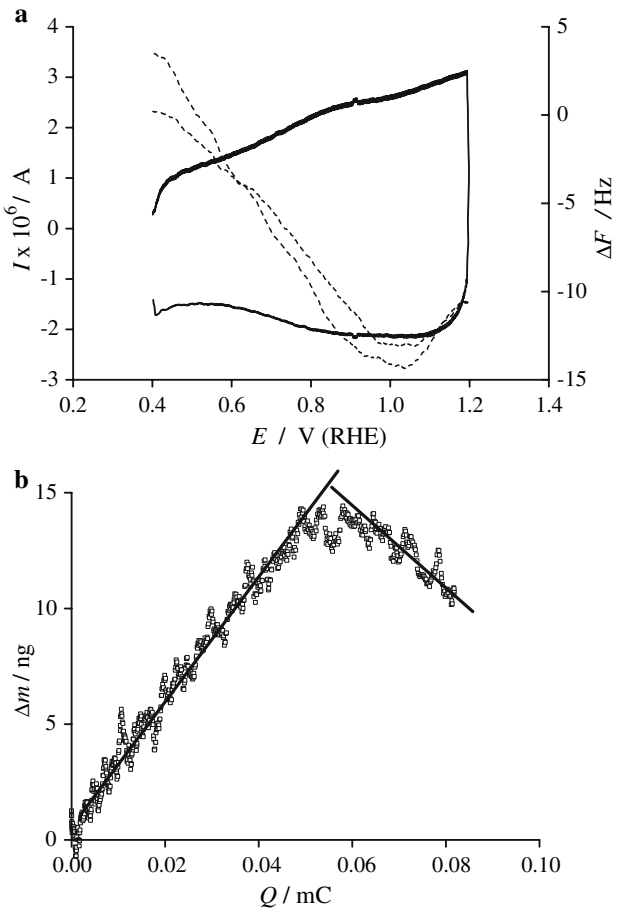

Fig. 5 (**a**) Current intensity (left axis, full line) and frequency variation (right axis, dashed line) versus E characteristics, recorded simultaneously, of a gold tip covered with $Ir_{0.15}Sn_{0.85}O_2$ in H_2SO_4 0.05 M; scan rate 20 mV s^{-1}. (**b**) Mass variation (Δm) versus cumulative charge (Q) obtained by integrating the CV of Fig. 5a

expulsion of 1 mol of H_3O^+ (theoretically − 19 g (mol of electrons)$^{-1}$) per mole of electrons. After 0.06 mC, a negative slope of −174 ng mC^{-1} is clearly observable, which points to a mass loss of 17 g (mol of electrons)$^{-1}$, that is compatible with the expulsion of 1 mol of H_3O^+ per mole of electrons. Then, the sulphate adsorption on the oxide surface seems to stop at potentials lower than the onset of OER. This feature is still under investigation, to elucidate the possible role of the anionic partner under both proton exchanging and oxygen evolving conditions.

When the $Ir_{0.15}Sn_{0.85}O_2$ modified gold tip is cycled in $HClO_4$ 0.1 M, a continuous mass decrease during the anodic sweep and an increase during the cathodic one are observed. Typical current and frequency variation with potential are presented in Fig. 6a: I vs. E displays the well known features of an Ir-based mixed oxide, i.e. broad peaks between 0.8 and 0.9 V due to (1), while the frequency variation is monotonic in the whole region of the charge/discharge process. The slope of −194 ng mC^{-1} for mass

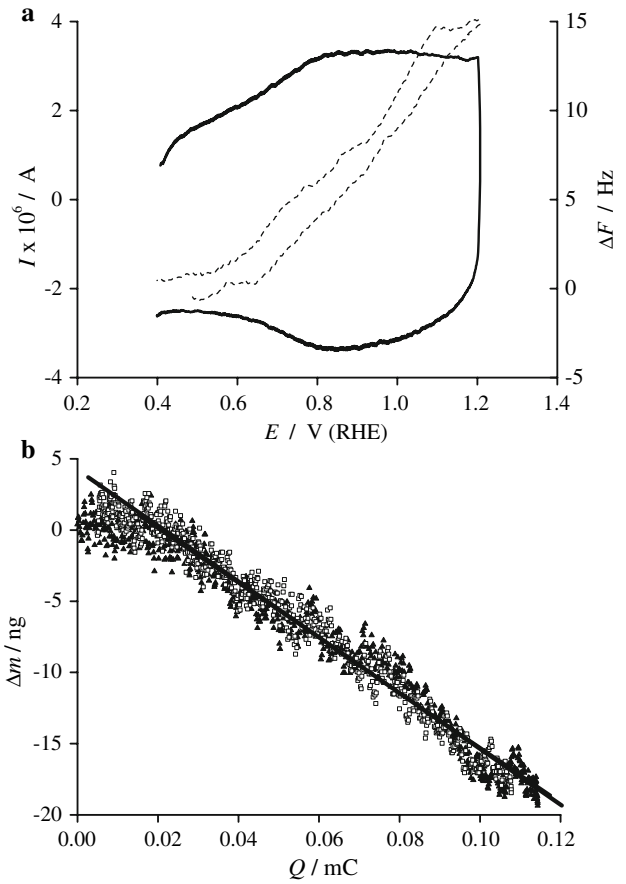

Fig. 6 (**a**) Current intensity (left axis, full line) and frequency variation (right axis, dashed line) versus E characteristics, recorded simultaneously, of a gold tip covered with $Ir_{0.15}Sn_{0.85}O_2$ in $HClO_4$ 0.1 M; scan rate 20 mV s^{-1}. (**b**) Mass variation (Δm) versus cumulative charge (Q) obtained by integrating the CV of Fig. 6a; empty squares: anodic scan; full triangles: cathodic scan

variation versus cumulative charge, Fig. 6b, points to the expulsion (anodic sweep) and insertion (cathodic sweep) of 1 mol of H_3O^+ per mole of electrons. Different batches of the same powder presented similar behaviours, although with reduced slopes, thus implying reduced hydration of the transferred protons. In connection with this, it is worth noting that the hydration capabilities of these kinds of powder are usually fully developed only after prolonged treatment under oxygen evolution conditions [34], a procedure not applicable in the present case, since it would detach particles from the tip.

The different behaviour of $Ir_{0.15}Sn_{0.85}O_2$ modified tips in the two acidic solutions supports the occurrence of stronger interactions between the mixed oxide and SO_4^{2-}, rather than ClO_4^-. This phenomenon is very likely connected with the intrinsic differences between the two anions, namely the large, low charge density perchlorate and the small, high charge density sulphate.

4 Conclusions

The combined use of EQCM and CV measurements was applied to investigate the properties of the mixed oxide electrocatalytic powder $Ir_{0.15}Sn_{0.85}O_2$ in the pseudo-capacitance region, 0.4 to 1.2 V versus RHE, in sulphuric and perchloric acid aqueous solutions.

The preliminary characterization of the bare Au tip in the same potential range (0.4–1.2 V versus RHE) and in a wider one (0.4–1.7 V versus RHE) was performed in both electrolytes. The extension of the positive end point into the full oxide formation and growth region has an etching effect on the gold surface. This activation, however, rapidly decreases after a few hours of exposure to either air or testing solution. The more evident consequence of this deactivation is the complete absence of electrolyte anion adsorption/desorption peaks and of concomitant mass variations, in the restricted potential window. Therefore, any contribution from exposed Au surface to the signals recorded in the presence of the electrocatalyst can be ruled out.

The EQCM response on the supported $Ir_{0.15}Sn_{0.85}O_2$ nanoparticles at sweeping potential provides insight into the chemical processes governing the proton exchange, pseudo-capacitance reaction. In particular the deinsertion/insertion of hydrated protons is observed during the positive/negative going sweeps, respectively. In addition, in sulphuric acid solutions, the adsorption/desorption of sulphate anions partially masks the pseudo-capacitance process. At $E > 1$ V, SO_4^{2-} definitely ceases to be adsorbed, revealing the proton exchange reaction. The observed H_2O/H^+ ratio ranges from 0.33 to 1, thus pointing to a higher hydration degree of the proton compared to the primary hydration sphere in aqueous solutions, and to a parallelly good hydration degree of the powder. The net increase in current intensity with respect to the Au support is certainly connected with the high surface area of the deposit, which consists mainly of round-shaped particles of 10–20 nm diameter, selectively sampled thanks to the tip preparation procedure. This ensures, on one hand, the conditions for good adherence, high compactness and low roughness required by the Sauerbrey equation for the frequency-to-mass conversion; and amplifies on the other hand all the electrode phenomena. This is consistent with a well hydrated interfacial region, in which acid/base equilibria can easily modify the charge of the defective surface sites, in concomitance with the transition from the less acidic Ir(III) to the more acidic Ir(IV) oxide, thus favouring the expulsion of the sulphate anions.

Acknowledgements The financial support by the Oronzio e Niccolò De Nora Foundation, MUR-The University of Milan (FIRST funds)

and Fondazione Monte dei Paschi di Siena are gratefully acknowledged.

References

1. Wuebbles DJ, Atul KJ (2001) Fuel Process Technol 71:99
2. Chalk SG, Miller JF (2006) J Power Sources 159:73
3. Ecsedy CJ, Murphy CG (1992) Water Environ Res 64:647
4. Alejaldre C, De Marco F, Finzi U et al (2005) Nucl Fusion 45:A1
5. Schultz MG, Diehl T, Brasseur GP, Zittel W (2003) Science 302:624
6. Dunn S (2002) Int J Hydrogen Energy 27:235
7. Turner JA (2004) Science 305:972
8. Stavy M (2005) J Sol Energy Eng 127:161
9. Hetland J, Mulder G (2007) Int J Hydrogen Energy 32:736
10. Granovskii M, Dincer I, Rosen MA (2007) Int J Hydrogen Energy 32:927
11. Schug CA (1998) Int J Hydrogen Energy 23:1113
12. Bilgen E (2004) Sol Energy 77:47
13. Ogden JM, Williams RH (1990) Int J Hydrogen Energy 15:155
14. Trasatti S (2001) Port Electrochim Acta 19:197
15. Rasten E, Hagen G, Tunold R (2003) Electrochim Acta 48:3945
16. Slavcheva E, Radev I, Bliznakov S et al (2007) Electrochim Acta 52:3889
17. De Pauli CP, Trasatti S (2002) J Electroanal Chem 538–539:145
18. Krstajic N, Trasatti S (1998) J Appl Electrochem 28:1291
19. Cardarelli F, Taxil P, Savall A et al (1998) J Appl Electrochem 28:245
20. Horvath E, Kristof J, Frost RL et al (2004) J Thermal Anal Calorim 78:687
21. Chen X, Chen G, Yue PL (2001) J Phys Chem B 105:4623
22. Comninellis Ch, Vercesi GP (1991) J Appl Electrochem 21:335
23. De Pauli CP, Trasatti S (1995) J Electroanal Chem 396:161
24. Lassali TAF, Boots JFC, Bulhoes LOS (1999) Electrochim Acta 44:4203
25. da Silva LA, Alves VA, de Castro SC, Boots JFC (2000) Colloid Surface A 170:119
26. Chen X, Chen G, Yue PL (2002) J Phys Chem B 106:4364
27. Ortiz PI, De Pauli CP, Trasatti S (2004) J New Mat Electrochem Syst 7:153
28. Chen X, Chen G (2005) J Electrochem Soc 152:J59
29. Marshall A, Børresen B, Hagen G et al (2007) Energy 32:431
30. Ardizzone S, Cappelletti G, Ionita M et al (2005) Electrochim Acta 50:4419
31. Ionita M, Cappelletti G, Minguzzi A et al (2006) J Nanopart Res 8:653
32. Minguzzi A (2004) Thesis, The University of Milan, Italy
33. Borgese L (2005) Thesis, The University of Milan, Italy
34. Ardizzone S, Bianchi CL, Cappelletti G et al (2006) J Electroanal Chem 589:160
35. Hu C-C, Chang K-H (2000) Electrochim Acta 45:2685
36. Sauerbrey G (1959) Z Phys 155:206
37. Vatankhah G, Lessard J, Jerkiewicz G et al (2003) Electrochim Acta 48:1613
38. Zolfaghari A, Conway BE, Jerkiewicz G (2002) Electrochim Acta 47:1173
39. Marshall A, Børresen B, Hagen G et al (2006) Electrochim Acta 51:3161
40. Tian M, Pell WG, Conway BE (2003) Electrochim Acta 48:2675
41. Watanabe M, Uchida H, Ikeda N (1995) J Electroanal Chem 380:255
42. Rodriguez Nieto FJ, Andreasen G, Martins ME et al (2003) J Phys Chem B 107:11452
43. Ardizzone S, Carugati A, Trasatti S (1981) J Electroanal Chem 126:287